energies

MDPI

Article

Optimising Flowback Strategies in Unconventional Reservoirs: The Critical Role of Capillary Forces and Fluid Dynamics

Hamid Reza Nasriani [1,*] and Mahmoud Jamiolahmady [2]

[1] School of Engineering & Computing, University of Central Lancashire, Preston PR1 2HE, UK
[2] Institute of Geoenergy Engineering, Heriot-Watt University, Edinburgh EH14 4AS, UK
* Correspondence: hrnasriani@uclan.ac.uk

Abstract: This study delves into the complexities of fluid cleanup processes post-hydraulic fracturing in unconventional gas deposits, focusing on the pivotal role of capillary pressure (P_c) correlations in tight and ultra-tight formations. Utilising Geo2Flow software, this research evaluates the efficacy of existing P_c models, identifying the Brooks and Corey model as notably precise for these formations, albeit recommending an adjustment to the pore size distribution index for a more accurate representation of rock behaviours. Further investigation centres on the cleanup process in multiple fractured horizontal wells, examining the impact of the P_c, matrix permeability, drawdown pressure, and fracturing fluid volume. A significant portion of this study addresses the influence of interfacial tension-reducing chemicals on post-fracturing production, highlighting their utility in ultra-tight formations, but advising against their use in tight formations due to environmental concerns and limited efficacy. The findings underscore the nuanced interplay between geological parameters and fracturing fluid dynamics, advocating for tailored fluid cleanup strategies that enhance the hydraulic fracturing efficiency while minimising the environmental impact. This comprehensive analysis offers valuable insights into optimising fracture cleanup and understanding the underlying physics, thereby contributing to more effective hydraulic fracturing practices.

Keywords: flowback cleanup; hydraulic fracturing; fracturing fluid; capillary pressure; IFT; unconventional reservoirs

Citation: Nasriani, H.R.; Jamiolahmady, M. Optimising Flowback Strategies in Unconventional Reservoirs: The Critical Role of Capillary Forces and Fluid Dynamics. *Energies* **2024**, *17*, 5822. https://doi.org/10.3390/en17235822

Academic Editors: Dameng Liu and Hossein Hamidi

Received: 22 February 2024
Revised: 13 June 2024
Accepted: 18 November 2024
Published: 21 November 2024

1. Introduction

The least polluting and emitting fossil fuel is thought to be natural gas. Due to its abundance and environmental sustainability, it is also regarded as one of the most significant energy sources for the future. Around the world, the use of natural gas is becoming increasingly significant for producing electricity, industrial processes, and domestic heating. The resources for natural gas are either conventional or unconventional. Despite being less economically viable than conventional natural gas reserves and more challenging to extract, there is a rising reliance on unconventional gas resources to meet the world's energy demands. Shale gas, gas hydrates, tight and ultra-tight gas sands, and coalbed methane are all sources of unconventional gas plays. The considerable rise in gas consumption has led to the development of further unconventional resources [1–3].

Fracturing, or hydraulic fracturing, is a prevailing technique for increasing the production of wells in unconventional gas reserves. With this technique, a rock formation is fractured by pumping a mixture of water, chemicals, and sand into a well under significant pressure. Different companies have widely adopted fracturing, which extracts large quantities of natural gas from unconventional deposits, but it has also been met with opposition due to environmental and health concerns [4–13].

Shale gas and tight gas sands are gaining popularity as unconventional resources. Conversely, conventional natural gas reserves are exhausted because of their availability and relative ease of access [14–20].

The potential benefits and disadvantages of unconventional natural gas resources need to be weighed against the larger picture of global energy demands and environmental concerns. The environmental impact of extracting unconventional gas resources and the possible health implications must be handled and examined, notwithstanding the resources' promise as a supply of natural gas. Companies and governments are developing new technologies and laws to meet energy demands while lowering their negative effects on the environment. Unconventional resources, thus, play a progressively essential role in addressing global energy demands, notwithstanding the difficulties they present compared to conventional reserves. Technologies and techniques, such as hydraulic fracturing, are being developed to enhance the production of unconventional gas resources while minimising the environmental impact. As the world continues to face energy challenges, it is crucial to consider the potential benefits and drawbacks of unconventional natural gas resources in the context of the bigger picture of global energy demands and environmental concerns [14–20].

Injecting large amounts of fracturing fluid, or FF, allows for the initiation and propagation of cracks in unconventional reservoirs [21–26]. In the tight oil and gas sectors, vertically drilled, hydraulically fractured wells were first drilled in Pennsylvania, a state in the northeastern United States. Numerous experimental, computational, and field studies have been conducted to determine how the hydraulic fracture cleanup effectiveness affects phase production in unconventional tight/ultra-tight formations [21,22]. Numerous field experiments have demonstrated that gas output can be considerably hampered by inadequate FF removal [27,28].

The physical characteristics of the FF, the formation's characteristics, and the hydraulic fracturing operation's design all affect the volume of the flowback. A total of 10 to 70 percent of the entire volume of the initially injected FF could make up for the flowback recovered from the surface of a well [29,30]. More FF is often retained in a formation. Therefore, when a formation has some micro fractures and higher matrix capillary pressures, the surface flowback recovery is reduced [29,30].

The oil and gas sector now emphasises optimising the fracturing fluid flowback for a number of purposes, such as maximising the net profit and addressing environmental concerns. Some techniques mitigate the FF flowback using a Tech-Flo hydraulic jet pump to maximise the load recovery [31]. Simultaneously isolating the hydrocarbon from a well stream helps hasten the safe recovery of a substantial amount of flowback. A flowback service for multiple fractured horizontal wells (MFHWs) in unconventional fields has also been made available by Halliburton [32]. CALIBR, a service offered by Haliburton, aims to boost well performance by reducing the completion damage and maximising the long-term output. The service enhances productivity and completion efficiency by continuously monitoring, analysing, and controlling the flowback. Through the use of CALIBR, hazardous flowback procedures can be avoided, the damage from fracture permeability can be reduced, and the performance of a well can be improved. This is achieved by continuously monitoring the well pressure, assessing the well performance, and adjusting the choke in real-time. CALIBR, a flowback operation service offered by Halliburton, enhances well performance by reducing the completion damage and maximising the long-term output. This service employs real-time monitoring and analysis using high-resolution pressure gauges like SPIDR®, allowing for precise adjustments to flowback processes based on continuous data acquisition. Each flowback plan is customised to a well's specific characteristics, incorporating its design, previous completion activities, and field knowledge to optimise productivity and minimise damage. Through an iterative process of continuous measurement, analysis, and choke adjustment, CALIBR avoids aggressive flowback strategies that could damage fracture conductivity, thus maintaining a well's performance. Additionally, the service mitigates potential damage-causing practices, reducing the risk of issues such as proppant washout and fines migration. Overall, CALIBR's comprehensive, data-driven approach to flowback management maximises the economic value and long-term productivity of wells [32]. Holditch [25] studied how the productivity of fractured wells is affected

by the growth of fluid saturation (FF), which is assumed to be water, and the reduction in permeability in the area near a fracture. His goal was to determine the impact of damage to the grid-like structure surrounding a fracture. He used a numerical simulator based on finite differences to conduct his research. It was found that in low-pressure drawdown conditions, where the drawdown pressure (DP) was only slightly greater than the capillary pressure (P_c) of the matrix in tight formations (reservoirs with low permeability), the effect of the capillary pressure was significant. He pointed out that water blocking takes place when the matrix permeability (km) around a fracture declines by 99.9%, or when the differential pressure (DP) is less than the capillary pressure (P_c) in the region where the fracturing fluid (FF) has penetrated. The invasion depth of the FF in their matrix extended up to 5 inches, and its distribution within the matrix adjacent to the hydraulic fracture was consistent. His study did not examine the impact of the FF volume on the conductivity of a fracture.

The decline in expected gas production is a complex process involving several factors, including matrix permeability damage caused by two-phase flow and the efficacy of cleaning up single fractured vertical wells. To understand these factors, researchers have conducted extensive studies that have shed light on the underlying mechanisms that affect gas productivity.

One important finding is that the P_c and K_r in the invaded zones are important factors for the cleanup effectiveness in low-permeability reservoir rocks. This conclusion was drawn by Pope et al. in 1996 [27], who determined a direct correlation between the gas flow and flowback recovery by analysing data taken from the field. They suggested that when liquid is produced from a hydraulic fracture, a corresponding space opens up, allowing for gas to flow towards a well. As the load recovery increases, the gas production also upsurges. To further investigate this, they examined the dependency of gas rates on the flowback, and advised that higher flow rates lead to higher load fluid recovery.

Following their investigation, Gdanski et al. [28] examined the formation damage caused by gas and fluid flow in the invaded zone and established a numerical model. They noticed that damages to the fracture sand face significantly lower the gas productivity if the permeability of the matrix in the invaded zone is reduced to 1% of the original permeability. However, they overlooked the fact that a higher P_c results in more fluid being absorbed into a matrix, which lowers the fluid saturation within a frack, increases the permeability of gas within a fracture, and produces cleaner fractures.

The next important factor for gas production is the effectiveness of the cleaning up of fractured wells. Ghahri et al. investigated this issue in 2010 [33], and showed that cleaning up such wells in gas fields efficiently enhances gas productivity. Their findings were based on numerical simulations and a detailed analysis of field data, and they proved that cleaning up single fractured vertical wells can lead to significant improvements in gas recovery.

These findings highlight the complex nature of gas production and the need to understand the underlying mechanisms that affect productivity. By building on the work of earlier researchers, current and future studies can continue to shed light on this important issue, aiming to improve gas recovery and meet the world's growing energy needs.

Additionally, the research has replicated the numerically developed model outcomes that Holditch (1979) indicated, which have since been used as a reference in several cleanup simulation investigations [25]. According to their findings, the presence of FF in a zone that has been invaded influences the total amount of gas recovery by diminishing the relative permeability of the gas, which reduces the gas rate when compared to a scenario in which FF was not pumped into a well. More significant FF recovery occurs during production when the FF viscosity is reduced and, as a result, the FF mobility is increased. They also emphasised that as the P_c rises, the FF penetrates deeper into a matrix, improving gas production and reducing the FF interference.

Ghahri et al. (2011) expanded on this study by thoroughly examining 16 important parameters while utilising an experimental design and a surface model [33]. They showed that the parameters relating to the FF cleanup within a fracture, particularly the kf, had a considerable impact on gas production loss, or GPL [33].

The central processing unit (CPU) time needed for these two numerical experiments was excessive [33]. As a result, the authors could only examine two simulation sets They conducted additional research on flowback cleanup processes. They simplified the model by reducing the number of parameters from 16 to 12 by removing four parameters that had a minimal impact on the cleanup performance. This made it easier to explore more diverse cleanup scenarios.

The study that was conducted by the same research team focused on different factors that included the size of the pores, the force between interfaces, how easy it is for substances to pass through the matrix and fracture, and the way that fluids move through these structures. The study was expanded to cover a wider variety of cleanup situations in gas reservoirs that are extremely tight. To achieve this, the researchers ran eighty-four simulations that considered various factors, such as the amount of fluid injected, the duration of the soak, the pressure at the bottom of the well, and the compactness of the formation [33].

The study revealed that the cleanup process becomes slower and the gas production loss becomes more significant as the formation becomes tighter (i.e., smaller km). Likewise, the study demonstrated that when the pressure drawdown is low, the capillary pressure (P_c) more significantly impacts the efficiency of the cleanup process than before. A similar result was obtained when the soaking period was increased. Nasriani and colleagues have conducted several studies on enhanced oil recovery, investigating various techniques and strategies [29,30,34–39], while more recent works by Modebelu et al. (2022) and Erimako et al. (2022) have focused on particular aspects of the process [40,41]. Nasriani et al. (2018) studied various factors impacting post-fracturing cleanup effectiveness [30,36]. The study considered several variables, such as the length of the fracture, well pressure, hysteresis, segregation due to gravity, mobility, immobility of the connate water, and the volume of the injected fracture fluid. The results of the investigation revealed that particular outcomes may arise when a considerable quantity of fracture fluid is injected into formations with extremely high permeability; it significantly reduces the gas flow and severely slows the cleanup procedure. Extending the soaking time or increasing the pressure drawdown does little to improve the GPL in this situation. The researchers found that hysteresis does significantly affect the efficiency of the cleanup process. The examination of cleanup performance was extended to explore the influence of layered systems, and it was discovered that the capillary pressure plays a more crucial role in the bottom layer than in the top layers. Additionally, the mobility coefficient of the fluid in a fracture is higher in the upper layer than in the lower layer. Furthermore, they suggested that using an IFT reduction agent during fracturing operations could reduce gas production losses in reservoirs with high water saturation levels.

Nasriani and Jamiolahmady (2019) expanded their research scope to include studies conducted to examine the cleanup procedure that takes place after hydraulic fracturing in wells with multiple horizontal fractures [29].

More precisely, the effect of wide-ranging horizontal lengths and fracture spacing in MFHWs on the cleanup efficiency was studied. Furthermore, the researchers compared the cleanup processes after fracturing in vertical wells (VWs) and MFHWs. Running the numerical simulations for the sets consumed considerable CPU time.

In an effort to mitigate the significant computational burden associated with simulation runs using a full factorial sampling (FFS) experimental design, and to accelerate the computational process, the researcher adopted an alternative approach known as Latin Hypercube Sampling (LHS). This novel sampling technique has emerged as a promising solution for conducting high-dimensional experiments with fewer runs, thereby reducing the overall CPU time required for simulations. They observed a difference in the trend

of the km values between the base reference set and the VW set for multiple fractured horizontal wells. The researchers identified that the shift in the flow geometry and well completion technique resulted in a shift in the trend of the km in the set to a positive coefficient value; previously, it was observed that the Km coefficient was negative in vertical wells. Additionally, they discovered that the capillary pressure (P_c) variables played a more crucial role in the sets, while the pertinent Corey parameters for the relative permeability models for both the gas and FF in both a matrix and fracture were further impactful in vertical wells.

According to these results, the FF production was more adversely impacted than the gas production in the set. In simpler terms, a greater P_c in MFHWs is more significant since it causes more FF to be more absorbed into the rock, and leads to less opposition to gas passage. It was also demonstrated that the MFHWs were cleaned up more quickly than the VWs. This resulted from their sets having a greater gas production rate. A slower (faster) cleanup was seen in reduced (increased) DP MFHW settings, comparable to those formerly reported for the related VW sets. They concluded that while the fracture interference and fracture spacing substantially impact the flow, they have little effect on the cleanup performance of MFHWs with varying spacing between fractures.

Recent advancements in hydraulic fracturing and unconventional gas extraction have significantly contributed to the efficiency and productivity of shale gas reservoirs. For instance, characterising anisotropic geomechanical properties through nanoindentation and upscaling approaches has provided a deeper understanding of formation behaviour, which is critical for optimising hydraulic fracturing treatments [42]. Additionally, computational analyses of proppant transport and screen-out phenomena have highlighted the complex interactions within fractures, leading to more effective fracturing strategies [43]. Experimental studies on the stable dispersion of coal fines during hydraulic fracturing flowback have emphasised the importance of addressing particle mobilisation to enhance the cleanup efficiency [44]. Furthermore, the probabilistic quantification of microparticle segregation under electrostatic forces has provided new insights into preventing screen-out during fracturing operations [45]. Innovative techniques, such as the co-application of indirect hydraulic fracturing and micro-proppants have improved the pre-drainage in low-permeability coals, highlighting the ongoing efforts to enhance gas recovery in challenging formations [46].

Moreover, the integration of machine learning into reservoir management has opened new avenues for predicting production and optimising resource extraction. Srinivasan et al. (2021) demonstrated the potential of machine learning-assisted history matching and production forecasting for shale gas reservoirs, which can significantly improve decision-making processes and operational efficiency [47]. These recent studies collectively underscore the critical role of technological advancements and interdisciplinary research in addressing the challenges of unconventional gas production, thereby helping to meet growing global energy demands while mitigating environmental impacts.

This study aims to enhance the existing knowledge of hydraulic fracturing treatments for real-world applications by building on prior research [3,14,15,20,30,31]. It specifically explores the influence of an unconventional P_c on the performance of MFHWs. This paper presents an in-depth analysis of P_c correlations applicable to tight and ultra-tight formations, utilising Geo2Flow software (https://geo2flow.net/). Geo2Flow is an advanced numerical modelling framework that integrates petrophysical, geological, engineering, and geophysical data to accurately simulate groundwater flow and solute transport in porous media. By matching 3D saturations to well logs, calculating precise 3D permeabilities, and identifying reservoir compartments, Geo2Flow enhances the accuracy of reserve estimations and subsurface models. Its interdisciplinary approach and robust algorithms ensure that it handles both data-rich and data-poor environments effectively, making it a valuable tool for environmental engineers and researchers [48].

An analysis of the P_c model, applied to 200 datasets from conventional, tight, and ultra-tight formations, proves that the Brooks and Corey model, with just one specific parameter, effectively represents the P_c data for unconventional plays. The results of this research recommend constraining the pore size distribution index (λ) to a 0.3–1.5 range for a more accurate portrayal of unconventional rock properties. The updated λ range is incorporated into the model to more accurately represent the unconventional P_c characteristics.

Additionally, for these five datasets, a novel dimensionless terminology—analogous to the gas production loss (GPL)—is introduced to study the influence of similar key parameters on FF production, which is a significant factor in the HF of unconventional reservoirs.

2. Methodology

A flowchart was used in this part to clarify the adopted analysis methodologies and terminologies, as shown in Figure 1. A comprehensive assessment of the capillary pressure (P_c) correlations for tight and ultra-tight formations was conducted. This analysis utilised Geo2Flow software to examine the dependability of existing P_c correlation models specifically for these formations [41,48]. Then, it was decided that the P_c data would be best represented by Brooks and Corey's model in unconventional plays. However, we proved, for the first time, that the λ range for unconventional resources used in the Brooks and Corey model must be adjusted to 0.3 to 1.5, rather than the 1 to 4 used in previous works [30]. This P_c formulation adjustment improved the capillary forces' representation in unconventional tight/ultra-tight rock formations and made it more realistic. Then, a multiple horizontal fractured well model initially created by [29] was utilised for the sets. The dimensions of the model are shown in Table 1; the validation procedure for the modified MFHW model is discussed elsewhere [30].

Table 1. MFHW model.

Lf (m)	wf (m)	Horizontal Length (m)	Number of Fractures	Xres (m)	Yres (m)	Zres (m)
90	0.004	600	7	2000	2000	40

Once the MFHW model was validated, five scenarios were considered. The five different scenarios are as follows:

Scenario 1. The base reference set.
Scenario 2. A set with a modified Lambda range.
Scenario 3. A set with a different injected FF.
Scenario 4. A set with a different Km range.
Scenario 5. A set with a larger drawdown.

It should be highlighted that each set consisted of 1000 simulation runs in which the 12 pertinent parameters were varied within their variation ranges. The ranges of all the pertinent parameters are shown in Table 2. A full explanation of the sampling approaches used in this work can be found elsewhere [29]. All the scenarios used Latin Hypercube Sampling (LHS) to generate the required simulation runs, and then a mathematical surface methodology was used to match an accurate model to the results from each set. Finally, the results from these sets were examined. A list of the sets that were analysed is shown in Table 3.

Figure 1. The workflow of this study.

Table 2. Parameters' variation ranges.

Parameter	Min	Max
k_f (D)	1	30
k_m	1 µD	100 µD
λ	1	4
IFT (mNm/m)	2	50
n_{gm}	1.5	5
n_{wm}	1.2	4
k_{maxg}	0.5	1.0
k_{maxw}	0.05	0.6
n_{gf}	1.5	5
n_{wf}	1.2	4
k_{maxg}	0.5	1.0
k_{maxw}	0.1	0.75

Table 3. MFHW set analysed.

Set Name	No. of Fracks	Horizontal Length (m)	DP (Psi)	FVR	Shut-In Time (Days)	k_f (D)	k_m (μD)	Lam	Sampling Approach	Number of Runs
Default Values	7	600	1000	2	2	1–30	1–100	1–4	LHS	1000
Set 8	✓	✓	✓	✓	✓	✓	✓	✓	✓	✓
Set 30	✓	✓	✓	✓	✓	✓	✓	0.3–1.5	✓	✓
Set 31	✓	✓	✓	✓	✓	✓	0.01–1	✓	✓	✓
Set 32	✓	✓	✓	10	✓	✓	✓	✓	✓	✓
Set 33	✓	✓	4000	✓	✓	✓	✓	✓	✓	✓

"✓" means the same value as the base case scenario, if a value is given it means a new value is considered instead of the default value in the base case scenario.

2.1. An In-Depth Assessment of the P_c Formulas for Unconventional Plays

This section presents the findings from a comprehensive analysis of different P_c correlations applied to unconventional formations, utilising Geo2Flow software [39]. For this research, 200 P_c datasets, collected from tight and ultra-tight formations in western U.S. basins were examined, with the measurements provided by the University of Kansas Center for Research and presented to the U.S. Department of Energy [40].

This study specifically examined various J-function models to investigate capillary force irregularities in tight and ultra-tight sands. This part discusses the initial and adapted Leverett J-functions, other J-function models, and the associated fit error indicators as applied to these unconventional formations.

2.1.1. The Leverett J-Function

Leverett (1941) [49] showed that in reservoir rocks with an identical lithology but varying porosity and permeability, the capillary pressure could be normalised using a single function, known as the Leverett J-Function. Rather than plotting the P_c against the S_w, Leverett instead used the J-Function, as detailed in Equation (1)

$$J(S_w) = \frac{P_c}{\gamma \cos\theta}\sqrt{\frac{k}{\varphi}} \quad (1)$$

where γ is the surface tension, θ is the contact angle, k is the permeability, and φ is the porosity.

According to Leverett's method, a small set of J-functions can effectively represent the P_c characteristics across the rocks within an entire reservoir. Leverett's findings imply that, for a specific rock type, most P_c curves can align with one J-function. Essentially, one J-function can encompass multiple P_c curves.

2.1.2. J-Function Displacement, J_d

The threshold value that the non-wetting phase must surpass to penetrate the rock is represented by the J-function displacement, J_d. This value aligns with the displacement pressure, P_d (also referred to as the threshold pressure, P_e), as will be outlined later in Equation (9) or the P_c curve. When the P_d is substituted into Equation (10), the J_d is obtained. In this study, all the P_c functions are dependent on the J_d, as it establishes the location of the fluid contacts.

2.1.3. The Model Proposed by Thomeer

In 1960, Thomeer [42] demonstrated that plotting the logarithm of the capillary pressure against the logarithm of the saturation of the non-wetting phase produces a hyper-

bolic curve. He introduced a J-function model, detailed in Equation (2), to represent this relationship.

$$S = 1 - 10^{-(\frac{G}{\mathrm{Log}(\frac{J}{J_d})})} \quad (2)$$

where S is the reduced saturation, J_d is the J-function displacement, J is the J-function value, and G is the pore geometric factor.

2.1.4. The J-Function Model Proposed by Brooks–Corey

Brooks and Corey (1966, 1964) developed a model using a bundle of capillary tubes to characterise a porous media, introducing the following terms [50,51]:

$$S = (\frac{J_d}{J})^{\lambda} = (\frac{J_d}{J})^{1/a_0} \quad (3)$$

Equation (3) corresponds to Equations (1) and (2) for the capillary pressure curve.

2.1.5. The J-Function Model Proposed by Bentsen–Anli

Bentsen and Anli (1977) suggested a J-function model expressed by Equation (4) [52].

$$S = e^{(\frac{J_d - J}{a_0})} \quad (4)$$

2.1.6. The Model of Skelt–Harrison

Skelt and Harrison (1995) proposed a J-function model characterised by two specific parameters, detailed in Equation (5) [46]. In contrast to the previous models, this model uniquely incorporates two parameters: a_0, serving as the scaling factor for the P_c, and a_1, which functions as the exponent for the scaled P_c.

$$S = 1 - e^{-(\frac{a_0}{J - J_d})^{a_1}} \quad (5)$$

Skelt and Harrison first presented their model for relating the height above the free water level and the P_c. Reformulating this relationship through the J-function yields Equation (5).

2.1.7. O'Meara Unimodal J Approach

Similar to the Skelt–Harrison J-function model, the O'Meara Unimodal J-function model incorporates two distinct parameters, a_0 and a_1, and is represented by Equation (6).

$$S = \frac{1}{2}\mathrm{erfc}(\frac{\mathrm{Log}(\frac{J - J_d}{a_0})}{a_1}) \quad (6)$$

In O'Meara's model, the erfc function denotes the complementary error function. This model is characterised by two distinct parameters: a_0, which signifies the median of the associated lognormal distribution, and a_1, which indicates the variance of that distribution.

2.2. Analysis of P_c Correlations

To evaluate the appropriateness of the specified P_c correlations for ultra-tight rocks, 200 P_c datasets were integrated into Geo2Flow. In Geo2Flow software [39], the data fit quality is determined through either the least absolute deviations approach or the least squares technique, with both assessed by an 'error in fit'. This error metric, applied to n data points (x_i, y_i) following the function y = f(x), is calculated as the sum of the squared

deviations between the actual data points and their corresponding values when using the least squares method, as outlined in Equation (7):

$$\Delta = \sum_{i=1}^{n} [y_i - f(x_i)]^2 \quad (7)$$

In the case of the least absolute deviations (LADs) approach, the error is defined as the total of the absolute differences between the data points and their respective corresponding values, as indicated by Equation (8):

$$\Delta = \sum_{i=1}^{n} |y_i - f(x_i)| \quad (8)$$

Notably, a lower Δ value indicates an improved curve fit. This work utilised the least squares method (LSM). For this task, all the datasets were initially formatted in Excel to align with the requirements of Geo2Flow before importing them into the software. Five different models were examined. Figure 2 illustrates the imported P_c datasets in relation to the saturation, with the P_c expressed in Bar. The corresponding J-functions, derived using specific K, φ, IFT, and contact angle values, are displayed in Figure 3.

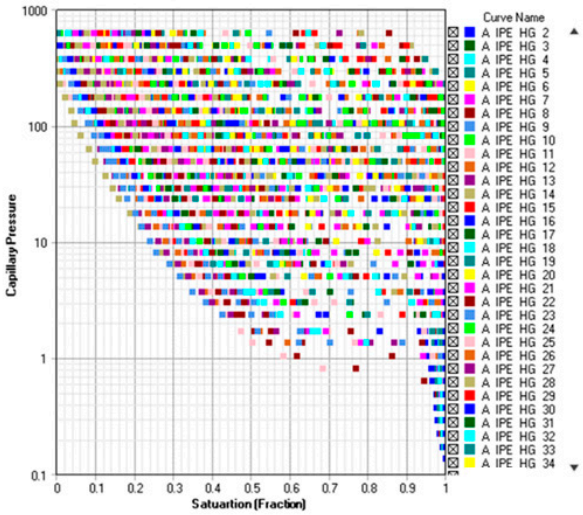

Figure 2. Two hundred P_c datasets vs. saturation (P_c in Bar).

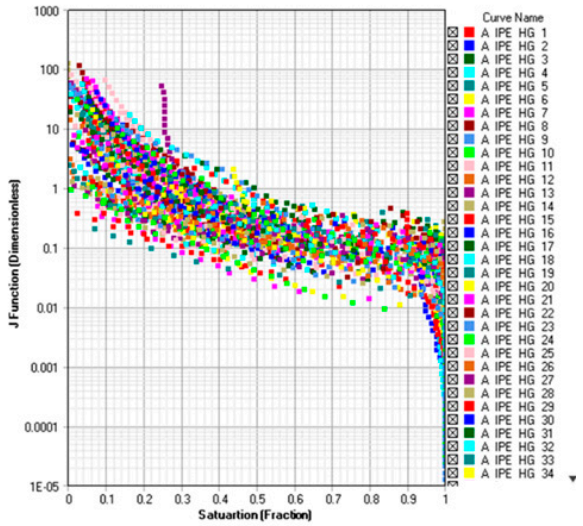

Figure 3. J-functions vs. S_w.

Five different models were evaluated as follows: three single-parameter models (Brooks and Corey, Thomeer and Bentsen, and Anli) and two dual-parameter models (Skelt–Harrison and O'Meara Unimodal). The P_c datasets were fitted using the least squares method (LSM), with the associated fit error values for each model outlined in Table 4. For the full dataset, Table 4 presents the error values for the five models. The Thomeer model, notably, provided the most accurate fit, while the Bentsen and Anli model had the highest error when assessing all the data. The models with dual parameters generally produced more precise P_c predictions due to their greater adaptability; however, the Thomeer model, despite being a single-parameter model, performed better than many others. The Brooks and Corey model was the second most accurate among the single-parameter models. To improve the assessment of these models' reliability in unconventional formations, the P_c datasets were divided into three categories: conventional (k > 0.1 md), tight (0.001 < K < 0.1 md), and ultra-tight (K < 0.001 md), with the conventional datasets being excluded from further analysis. The LSM was reapplied to the unconventional data, and the resulting error values for each model are shown in Table 4. For the tight P_c data, Table 4 includes the error values for the Thomeer, Brooks and Corey, Bentsen and Anli, Skelt–Harrison, and O'Meara models. The Brooks and Corey model was found to be the most accurate among the single-parameter models, while the Skelt–Harrison model performed best among the dual-parameter models. For the ultra-tight P_c data, the error values in Table 4 indicate that the Brooks and Corey model, along with Thomeer's, were the best-performing single-parameter models, while the Skelt–Harrison and O'Meara Unimodal were superior among the dual-parameter models. Table 4 also shows that the Bentsen and Anli model was the least accurate for both the tight and ultra-tight P_c datasets, while the Brooks and Corey model was the most effective for these unconventional categories.

Table 4. Error-in-fit analysis.

	J Function Model Name	Error in Fit for All P_c Datasets	Error in Fit for Tight P_c Datasets	Error in Fit for Ultra-Tight P_c Datasets
Models with one model-specific parameter	Thomeer	6.26×10^{-3}	9.97×10^{-3}	2.89×10^{-2}
	Brooks and Corey	8.91×10^{-3}	8.64×10^{-3}	2.91×10^{-2}
	Bentsen and Anli	1.49×10^{-2}	1.21×10^{-2}	2.95×10^{-2}
Models with two model-specific parameters	Skelt-Harrison	6.68×10^{-3}	7.86×10^{-3}	2.87×10^{-2}
	O'Meara Unimodal	7.09×10^{-3}	8.49×10^{-3}	2.86×10^{-2}

2.2.1. Evaluation of the Brooks and Corey Model

The results demonstrate that the Brooks and Corey model effectively fits both the tight and ultra-tight datasets. The evaluation of five distinct J models was conducted for the P_c datasets for tight formations (0.001 md < K < 0.1 md) and the P_c datasets for ultra-tight formations (K < 0.001 md), as described in previously. A range of datasets from these categories were analysed. For each dataset, the Brooks and Corey model was applied to ascertain the typical λ characteristic of these unconventional datasets. The findings show that the Brooks and Corey model accurately represents both the tight and ultra-tight datasets.

Table 5 displays a selection of the evaluated data, detailing the sample dataset names, K, φ, estimated λ, J-function displacement, and curve-fitting error metrics. The estimated λ for these samples spans from 0.313 to 1.49. To demonstrate the high correlation between the Brooks and Corey model and the observed data, two specific sample datasets were chosen as follows: a tight and an ultra-tight dataset.

Table 5. The λ analysis.

Sample Data Set Name	Permeability, md	Porosity %	λ	J_d	Error in Fit
A-IPE-HG-195	0.0086	11.8	1.080	0.0540	2.06×10^{-3}
A-IPE-HG-120	0.00062	5.5	0.462	0.0326	3.23×10^{-5}
A-IPE-HG-141	0.0011	12.8	1.062	0.0228	8.80×10^{-4}
A-IPE-HG-142	0.0062	7.3	1.042	0.0377	1.40×10^{-3}
A-IPE-HG-112	0.008	10.5	1.179	0.0546	2.01×10^{-4}
A-IPE-HG-114	0.00957	10.2	1.497	0.0703	8.60×10^{-4}
A-IPE-HG-128	0.0199	12	0.458	0.0555	4.63×10^{-4}
A-IPE-HG-168	0.0364	9	0.613	0.0776	5.50×10^{-4}
A-IPE-HG-77	0.0416	9.5	0.386	0.0345	7.41×10^{-4}
A-IPE-HG-76	0.0512	9.8	0.492	0.0394	5.18×10^{-4}
A-IPE-HG-60	0.067	15.4	0.565	0.0827	2.79×10^{-4}
A-IPE-HG-101	0.0728	14.1	0.575	0.1242	3.16×10^{-4}
A-IPE-HG-167	0.0978	9.8	0.743	0.1016	1.99×10^{-4}
A-IPE-HG-9	0.137	11.4	0.556	0.0492	3.63×10^{-4}
A-IPE-HG-14	0.00016	3	0.670	0.0550	1.99×10^{-4}
A-IPE-HG-34	0.00025	4.5	0.766	0.0079	5.04×10^{-4}
A-IPE-HG-130	0.000064	8.2	0.694	0.0231	2.84×10^{-4}
A-IPE-HG-52	0.000343	5.5	0.704	0.0489	4.46×10^{-5}
A-IPE-HG-132	0.00028	4.2	0.951	0.0875	4.00×10^{-3}
A-IPE-HG-137	0.000374	3.7	0.357	0.1016	1.36×10^{-3}
A-IPE-HG-19	0.00039	4.2	0.826	0.0560	7.43×10^{-4}
A-IPE-HG-93	0.00025	7.8	0.664	0.0348	7.17×10^{-4}
A-IPE-HG-27	0.00021	4.3	0.487	0.0173	5.43×10^{-4}
A-IPE-HG-31	0.00034	5.7	0.475	0.0493	7.57×10^{-6}
A-IPE-HG-110	0.00117	8.4	0.513	0.0341	7.42×10^{-4}
A-IPE-HG-55	0.000088	3	0.749	0.0500	7.31×10^{-4}
A-IPE-HG-37	0.00227	10.2	0.538	0.0252	1.13×10^{-4}
A-IPE-HG-109	0.00029	4	0.313	0.0351	1.18×10^{-4}
A-IPE-HG-118	0.0189	10.2	0.921	0.0525	6.27×10^{-5}
A-IPE-HG-119	0.00247	9.7	0.561	0.0320	2.36×10^{-4}

A data point from the tight data group had a permeability (K) of 0.0086 md and a porosity of 11.8%, with an error in fit of 2.06×10^{-3}, indicating minimal deviation. Figure 4 illustrates the close match between the Brooks and Corey model fit and the actual data for this set, showing a λ of 1.08 and a J-function displacement of 0.054. The ultra-tight sample had a permeability (K) of 0.00016 md and a porosity of 3%, with an error in fit of 1.99×10^{-4}, suggesting an excellent fit. Figure 5 illustrates the almost exact alignment between the Brooks and Corey model fit and the observed data, characterised by a λ of 0.67 and a J-function displacement value of 0.055.

2.2.2. Concave-Down Effect

Certain P_c (or Leverett J) curves exhibit a concave-down section where dead volume errors become evident when the apparent P_c displacement, or the related displacement value for the J-function, is noted at a wetting phase saturation below 1. Figure 6 highlights this dead volume error in a dataset. For wetting phase saturations between 1 and 0.97, some of the data points indicate that the non-wetting phase can more readily penetrate the rock. However, when the J-function value exceeds 0.04, the curve characteristics shift, making it harder for the non-wetting phase to enter. At this threshold, a discontinuity or change in the curve shape occurs, which the Brooks and Corey model cannot capture, linking it to the dead volume errors in the P_c measurements. Hence, this effect should be adjusted to avoid it being mistakenly interpreted as a change in rock characteristics, as illustrated in Figure 7.

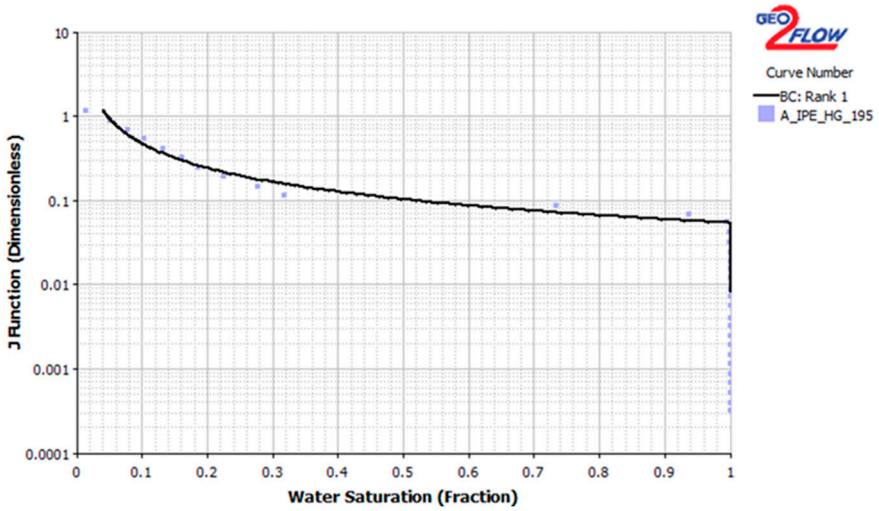

Figure 4. Comparison of actual and matched J-functions against S_w for P_c sample dataset from tight sets.

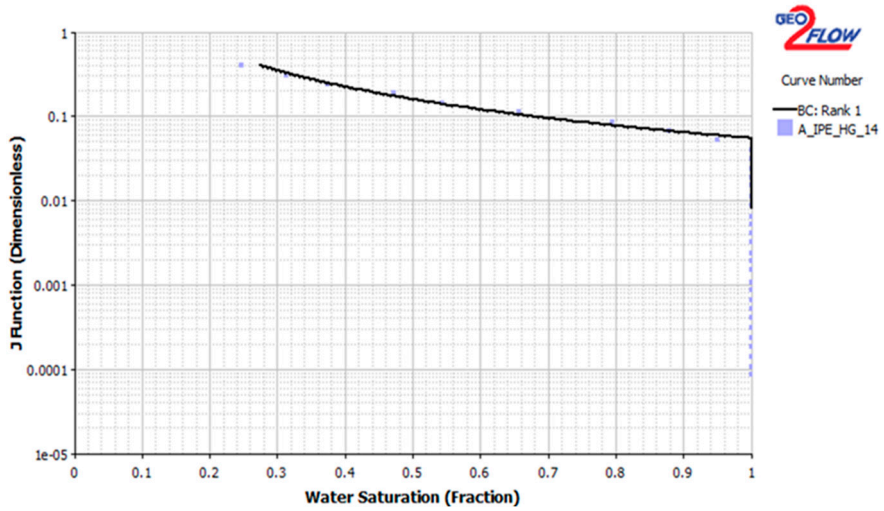

Figure 5. Comparison of actual and predicted J-functions against S_w levels for P_c sample dataset from ultra-tight formations.

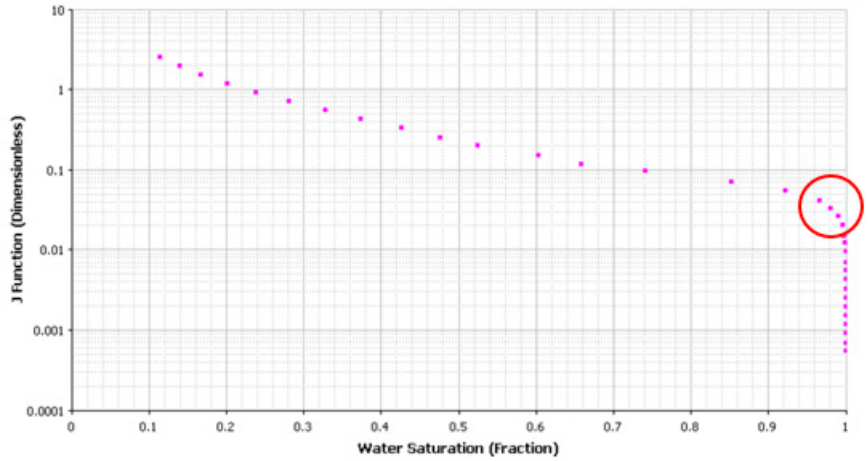

Figure 6. P_c sample dataset with dead volume error (red circle indicates the concave down trend).

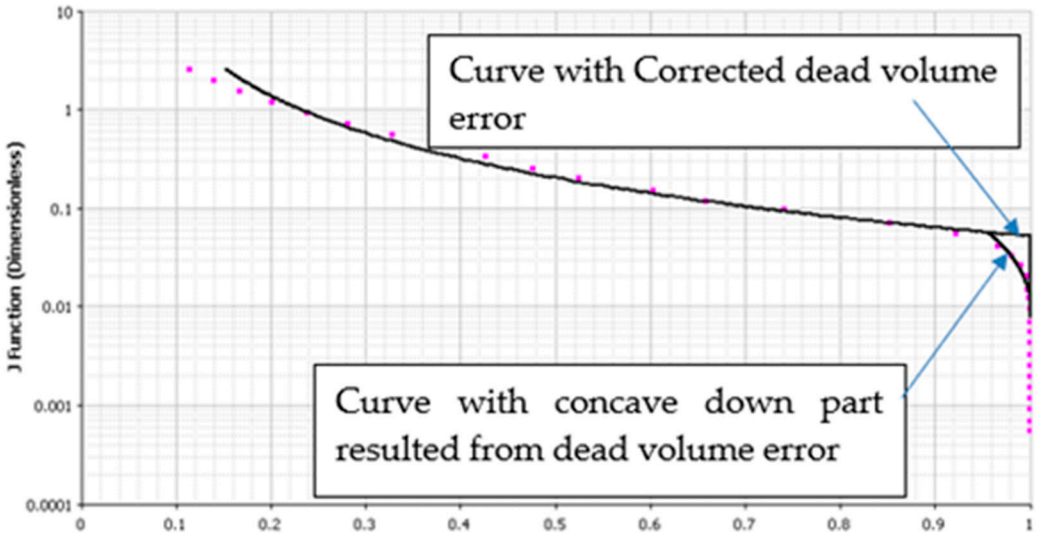

Figure 7. P_c data sample adjusted for dead volume errors.

In P_c studies, the dead volume is defined as the quantity of a fluid (such as mercury) that is presumed to fill the core sample but is, in reality, retained within the core holder or has penetrated the surface vugs or irregular features. According to Shafer & Neasham (2000) [53], this adjustment is known as the closure correction. In cases where a dead volume is identified, it is essential to modify the experimental data, as it fails to reflect the genuine capillary characteristics of the core sample.

These observations indicate that the Brooks and Corey model, with its single specific parameter, provides a simple yet accurate representation of P_c data in unconventional rocks. It is important to note that these findings are derived from core samples from basins in the western U.S., reflecting a specific range of properties. Furthermore, the findings of this research indicate that to effectively characterise the behaviours of unconventional tight and ultra-tight rocks, the λ needs to be limited to a range of 0.3 to 1.5. Previously, a broader index range (from 1 to 4) was applied in a MFHW cleanup study, which requires the adjustment to align with the findings presented in the following sections.

2.3. Developing, Modifying, and Validating the Model

The MFHW model was established using ECLIPSE 100 [54] to study the cleanup operation of multiple fractured horizontal wells. The equations and underlying physics utilised in Eclipse are thoroughly explained elsewhere [54]. Seven fractures were added to the 600 m long horizontal well in the new pre-fractured MFHW model. Instead of using a global refinement around the fractures, the MFHWs were built using local grid refinement (LGR). Using LGR allowed the authors to capture, with a minimal CPU time increase, the impact of changing the flow parameters in the SRV. The model's initial pressure was 7500 psi, and the average matrix porosity was 15%. The dimensions of the numerical models are shown in Table 1. The model is shown in Figure 8. The set numbers denote the sequence in which they were performed as a subset of a much larger set of simulations; not all are included in this article. During the post-fracturing stage of the numerical modelling, a controlled bottom-hole flowing pressure was applied to produce both gas and fracturing fluid (FF), which was found to be water. As shown in Figure 8, the fracture half-length is 90 metres, as mentioned in Table 1.

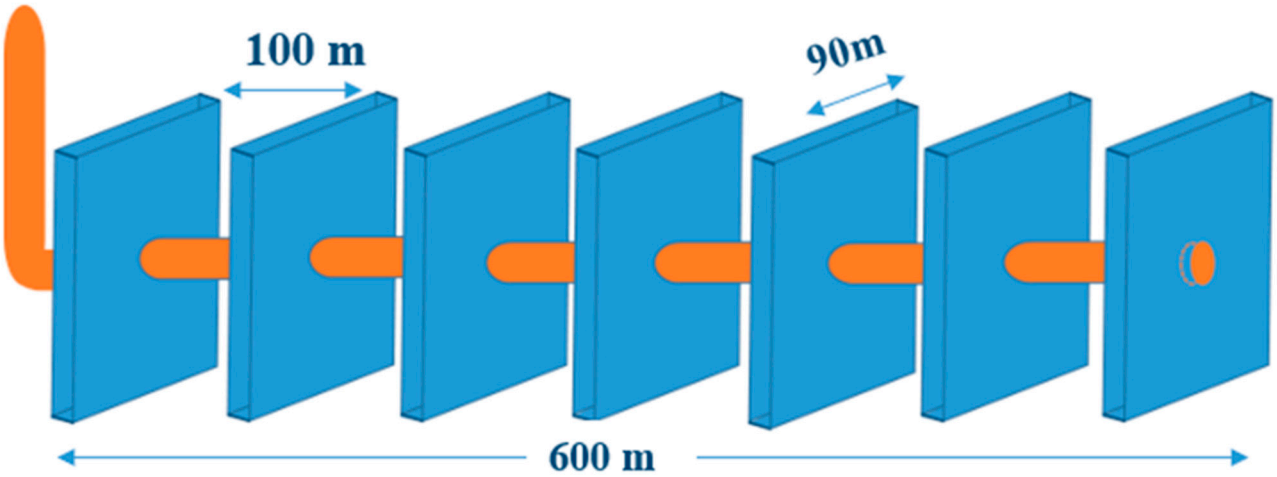

Figure 8. The modelled MFHW.

For the FF, the relevant compressibility and viscosity were calculated as 0.000005 (1/psia) and 0.5 cp, respectively. In the MFHW scenario's presumed base reference sets, the FF injected during the hydraulic fracturing stage was twice the volume of the fracture. It is important to note that a two-day period of well shut-in applied immediately after the FF injection and before flowback production. The method for validating the amended VW model and its governing equations was previously discussed [30]. To validate the MFHW model, the well pressures vs. production time estimated by the simulation were compared to what was observed in an analytical model for MFHWs [29].

Figure 9 compares the predicted well bottom-hole pressure (Pwf) by the simulation model with that by the analytical model as a function of production time. The fact that the two curves overlap and are stacked on top of one another supports the accuracy of the simulation model. It should be emphasised that this study takes into account twelve pertinent variables that have an impact on post-fracturing cleanup processes. The first eight values among the twelve parameters represent the exponents and endpoints of the Brooks–Corey relationship for Kr in two separate phases.

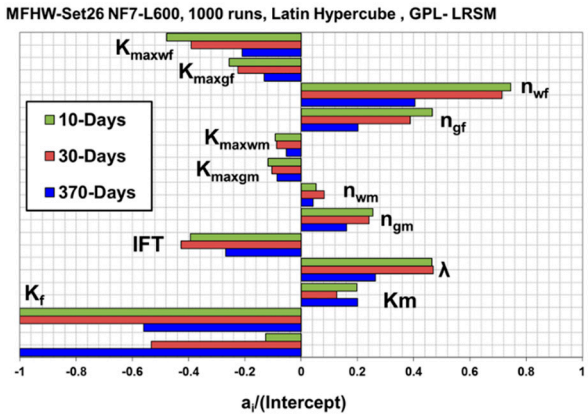

Figure 9. GPL tornado chart for base reference set.

The matrix's P_c is influenced by the Km, IFT, and λ (pore size distribution index). The final variable is Kf. Table 2 lists the possible variation ranges for the parameters. It should be noted that six of the parameters given in Table 2—namely, the DP, porosity of the matrix, and Swc and Sgc in both the fracture and matrix—are taken into consideration as constants throughout the simulation sets.

Equations (1) and (2) depict the capillary and threshold (entry) pressure, respectively [51,55]. Equations (3) and (4) establish the relationship between the gas and water

relative to the permeability, as formulated by Brooks and Corey in 1966. It is important to note that the data are generated using either FFS or LHS sampling techniques for each simulation set, drawing from the specified parameter ranges listed in Table 2.

$$\frac{Pd}{IFT} = 0.0075 \times K^{-0.5} \tag{9}$$

where

- IFT is the interfacial tension (IFT);
- Km is measured in mD.

$$\left(\frac{Pd}{Pc}\right)^{\lambda} = \frac{Sw - Swr}{1 - Swr} \tag{10}$$

$$k_{rw} = K_{maxw} \times \left(\frac{Sw - Swr}{1 - Swr - Sgr}\right)^{nw} \tag{11}$$

$$k_{rg} = K_{maxg} \times \left(\frac{Sg - Sgr}{1 - Swr - Sgr}\right)^{ng} \tag{12}$$

Table 3 shows various simulation sets for each DP to fully understand how the pressure drop (DP) affects the cleanup performance. The 12 relevant parameters in this study are scaled between 0 and 1, where 0 represents the lower bound and 1 represents the upper limit, making the assessment of the cleanup processes via the response surface approach more effective (RSM).

2.4. The Main Output and RSM

The gas production loss (GPL), expressed as a percentage, measures the effectiveness of the cleanup process. It is determined by calculating the difference in the cumulative fracture productions between a clean, undamaged fracture and an unclean, damaged fracture, and comparing it to the cumulative fracture productions of a clean, undamaged fracture.

$$GPL = 100 \times \left[\frac{FGPT_{clean} - FGPT_{unclean}}{FGPT_{clean}}\right] \tag{13}$$

where FGPT is the field gas cumulative production.

After a hydraulic fracturing operation, having a clean (undamaged) fracture is extremely difficult or technically impossible. In order to attain a much cleaner fracture and higher productivity, the current field tactics for fracturing operations could benefit from additional enhancements. This would require a comprehensive understanding of the parameters involved and their effects on post-fracturing activities. To facilitate the comparison of different instances, the response parameter of the GPL should be reported in a normalised format. The present work uses tornado charts to illustrate how the 12 previously listed characteristics affect the gas production loss. According to this technique, if a parameter positively affects the cleanup effectiveness, it reduces the gas production loss (GPL) or increases the total amount of gas produced while the parameter is increasing. In contrast, if a parameter harms the cleanup effectiveness, it will result in GPL or less cumulative gas production as its value increases. The response surface methodology is frequently used to examine how sensitive the several relevant parameters are to a specific major output. RSMs in statistics and mathematics uncover a true relationship between multiple independent variables, such as x_1, x_2, x_3, x_4, …, x_n, and the primary output (y or $f(x_i)$).

Equation (6) defines the RSM, often the polynomial that best fits the data.

$$y = a_0 + \sum_{k=1}^{n} a_k x_k + \sum_{i=1}^{n} \sum_{j=i+1}^{n} a_i a_j x_i x_j + \sum_{l=1}^{n} a_l x_l^2 \tag{14}$$

Equation (6) lists four distinct RSM models:

- An LRSM (Model for Linear Response Surface) with a_0 and $a_k x_k$.
- If a_0 and $a_k x_k$ are taken into account in addition to $a_i a_j x_i x_j$, then an LRSM with an interaction (ILRSM) will be used.
- A pure quadratic response surface model (PQRSM) that takes into account the quadratic terms a_0, $a_k x_k$, and $a_l {x_l}^2$.
- A full quadratic response surface model (FQRSM) transforms this into $(a_l {x_l}^2)$.

This study determines the GPL as a function of the 12 pertinent factors for the Latin Hypercube Sampling (LHS) approach using ILRSM and FQRSM models. A Python code is created to perform every simulation in a simulation set, including the pre-and post-processing stages of the fracturing procedure.

2.5. The Second Response Surface Model

During flowback, some of the injected fracture fluid (FF) returns as flowback. The FF volume that returns can vary greatly depending on the key parameters and the design of the fracture. The FF that is produced normally includes a combination of surface-returned FF, some formation brine, and a portion of the injected chemicals. Consequently, understanding the volume of produced water is critical. Managing the produced FF poses a significant challenge for the development and production of unconventional gas formations due to strict regulations concerning FF flowback, its environmental impact, and limited disposal options. These factors push operators to constantly review and adjust their hydraulic fracturing strategies and FF flowback management approaches. To address this, a new dimensionless term, the Produced Fracture Fluid (PFF), has been established. The influence of the key parameters, similar to those affecting the GPL, on the PFF has been examined. The PFF, which serves as the second response metric, indicates the proportion of flowback relative to the total injected FF during the fracturing process, determined by the following equation.

$$\text{PFF} = 100 \times \left[\frac{\text{The volume of produced FF or simply Field water production}}{\text{Total FF injected at fracturing stage (FF injection stage)}} \right] \quad (15)$$

2.6. Analysis Methodology

This study examines five distinct sets of MFHWs (each set consists of 1000 simulation runs). Table 3 lists each of these various sets in total. The fact that each set has a reservoir with identical dimensions should be emphasised. However, each set has a different P_c pertinent parameter (i.e., Λ), different pressure drawdown, matrix permeability, and FF injection volume. The 12 pertinent factors are considered by the base reference set, with the default ranges displayed in the table. When a parameter in Table 3 has a tick next to it, the parameter's default variation range is considered; otherwise, a new range of variation is established, and the name of the new set is determined based on the degree of dissimilarity between the range of parameter values and the set that was selected as the reference.

3. Results and Analyses

The previous and updated pore size distribution ranges relevant to the P_c for unconventional formations with varying Kmr, DP, and FVR are utilised. This approach aims to assess how these parameters influenced the cleanup efficiency when employing an unconventional P_c. The resulting data are examined, compared, and discussed in this section.

3.1. Unconventional Capillary Pressure

Two sets are created and analysed in this section. Set 8 is the base reference set with the dimensions and parameters' variation range shown in Tables 1 and 2. As mentioned previously, the MFHW is shown in Figure 8.

The updated λ range which corresponds to the P_c values for tight/ultra-tight formations is also used in Set 30 ($0.3 < \lambda < 1.5$),. Importantly, all the parameters and dimensions

align with those of Set 8, apart from the revised λ range. A comparison is made between the GPL tornado chart for Set 30, featuring the new λ range (0.3 < λ< 1.5, Figure 10), and the Set 26 base reference set (Figure 9). The comparison shows consistent trends across both charts for all the key parameters. Additionally, it is noted that in Set 30, with its lower λ range, the P_c-related parameters, particularly Λ, have a greater influence on the GPL. This increased influence is attributed to the narrower λ range in Set 30, which enhances the importance of the P_c values relative to Set 26.

$$K_m \downarrow,\ IFT \uparrow,\ \lambda \downarrow,\ S_w \downarrow \rightarrow P_c \uparrow$$

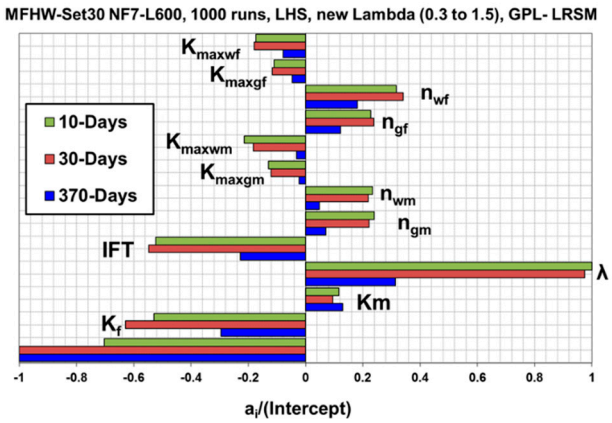

Figure 10. GPL tornado chart of effect of unconventional P_c.

The effect of fluid mobility, particularly water mobility, within the matrix is slightly more pronounced in Set 30 in contrast to Set 26, which has lower P_c values. This difference arises from the higher P_c of the matrix in Set 30, which hinders fluid mobility.

The tornado chart for the PFF relating to Set 26 is shown in (Figure 11). The tornado chart for the PFF relating to Set 30, utilising the updated λ range of 0.3 to 1.5 as shown in Figure 12, is in comparison to the chart for the Set 26 base reference set that includes a modified λ range (Figure 11). Both charts show a consistent trend across all the key parameters, exclusive of Kf: in Set 30, an increase in Kf led to a decrease in FF production (PFF), whereas the reverse effect was observed in Set 26. A new MATLAB (R20016b) code was developed, and the water saturation (Swat), as well as the values from the GRDECL file in Floviz for the end of the soaking period, were extracted and utilised. In an Eclipse simulation, a GRDECL file defines the grid structure and geometry, including the grid dimensions, coordinates, and properties. It is essential for setting up a simulation, as it provides the spatial framework for the reservoir model.

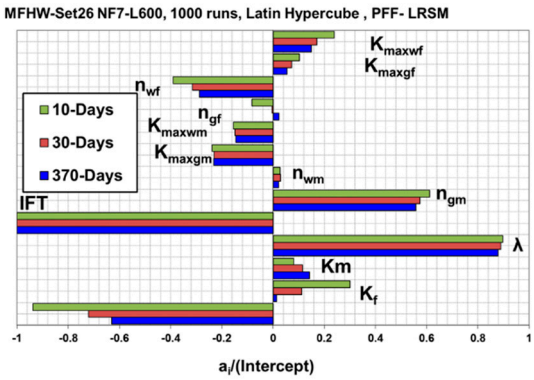

Figure 11. PFF tornado chart of base reference set.

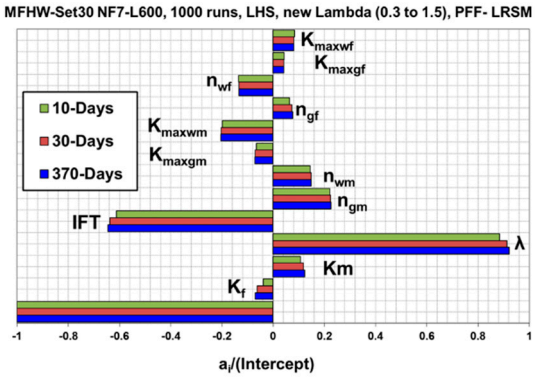

Figure 12. PFF tornado chart of effect of unconventional P_c.

To further investigate the observed shift in the Kf trend shown in the PFF tornado chart for Set 30, a run number of 29 was chosen, where Kf was set close to its maximum value. A S_w map was then created to visualise the water distribution at the end of the soaking period for this high-Kf scenario and to contrast it with the minimum-Kf scenario, in which Kf was set to its lowest value.

Examining Figures 13–15 highlights the significant contrasts between the Max-Kf and Min-Kf scenarios. In the Max-Kf scenario (Figure 13), a specific zone (Region B) within the first 45 m of the fracture's half-length from the well exhibits water saturation levels between 30% and 70%. Conversely, in the Min-Kf scenario (Figure 14), a considerable amount of fracturing fluid (FF) is either injected into or absorbed by the matrix, resulting in water saturation levels ranging from 60% to 100% (Region A) within approximately the initial 10 m of the fracture near the well. This disparity occurs because, during an FF injection, the fluid moves significantly faster and more freely through the fracture in the Max-Kf scenario compared to the Min-Kf case. This results in a more dispersed FF distribution, particularly within the matrix, in the Max-Kf scenario. Therefore, in the case of Min-Kf, a large volume of FF is infused or imbibed within a smaller matrix distance near the fracture (around 10 m), creating Region A, which has a higher water saturation (S_w) and a lower capillary pressure (P_c). This region is more easily replicated during the backflow phase than in the Max-Kf scenario.

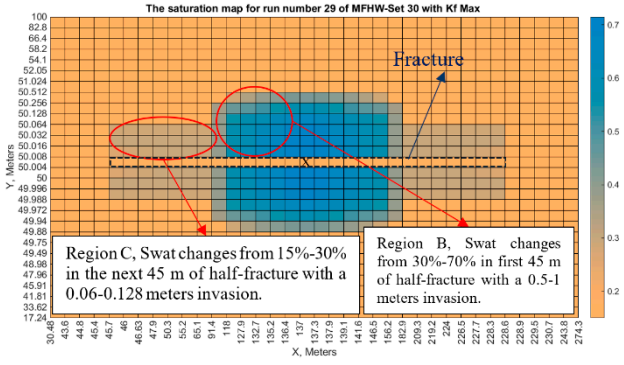

Figure 13. FF saturation distribution map for run No. 29, with Kf-max for Set 30 following a shut-in period.

The P_c is plotted in Figure 15 for Sets 26 and 30 (run No. 29) with different areas indicated in Figures 13 and 14. From Figure 15, it is evident that Set 30 generally displays significantly higher P_c values compared to Set 26. This difference is due to the narrower λ range in Set 30 (0.3 to 1.5) compared to Set 26 (1 to 4), leading to an increase in the P_c. Additionally, for Set 30, the P_c curve remains identical for both Kf-Max and Kf-Min.

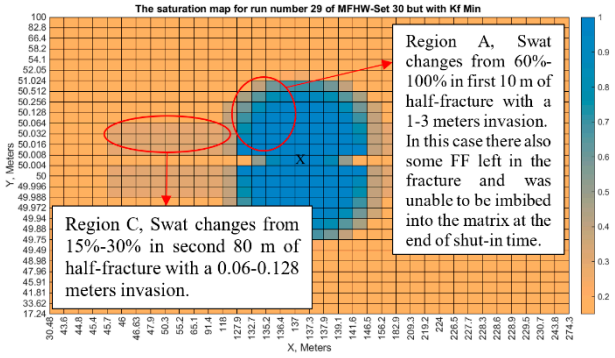

Figure 14. FF saturation distribution map for run No. 29, with Kf-min for Set 30 following a shut-in.

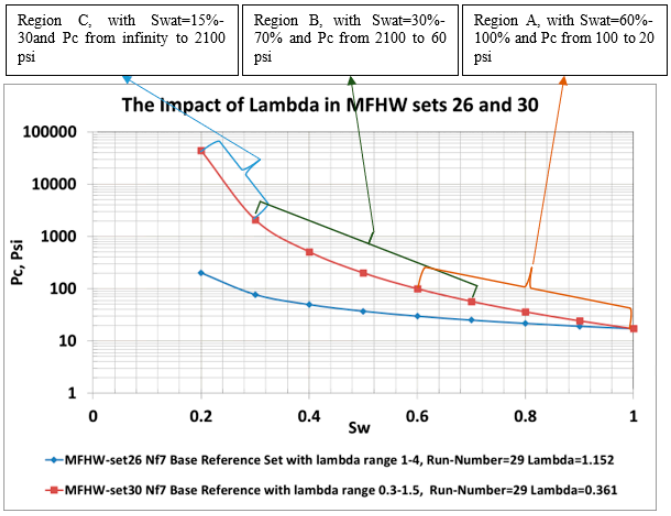

Figure 15. P_c, along with various regions discussed, is illustrated in Figures 13 and 14.

In Region A, where the water saturation ranges from 60% to 100%, the capillary pressure (P_c) spans from 100 psi to 20 psi for Set 30, and from 30 psi to 20 psi for Set 26. In Region B, with S_w levels between 30% and 70%, the P_c fluctuates between 2100 psi and 60 psi for Set 30, and between 80 psi and 25 psi for Set 26. Lastly, in Region C, where the water saturation is between 0% and 30%, the P_c decreases from infinity to 2100 psi for Set 30, and from infinity to 80 psi for Set 26.

Notably, Regions A, B, and C each exhibit distinct P_c values. Throughout the flowback period, a rise in FF production is noted, attributed to elevated S_w values and a reduced P_c, which signifies a decrease in the retained FF within the set featuring the lowest Kf. This explains the negative Kf value displayed in the associated tornado chart (Figure 12).

Kf influences FF production in two distinct ways:

1. As the value of Kf increases, the mobility of the FF within a fracture increases during the production stage necessary for increased production of the FF.
2. A higher Kf increases the FF fracture mobility during the injection phase leading to an improved distribution of the FF and reduced S_w values in the matrix and, hence, higher P_c values that hold additional FF during the production phase and, hence, less FF output.

In Set 30, the secondary influence of Kf is notably dominant, resulting in a shift in the trend of Kf in the PFF tornado chart for this set, as shown in Figure 12. Additionally, for Set 30, where the λ range varies from 0.3 to 1.5, the parameters related to the P_c, especially Λ, have the highest impact on the GPL. This is because the λ range of Set 27 is much narrower as compared to that for Set 26 and, therefore, the P_c values are much more sensitive.

An additional key observation from the PFF tornado charts for Sets 26 and 30 (Figures 12 and 13) is the inverse relationship between FF production and water mobility within a matrix. This is due to the dual effects of the matrix water mobility on FF production:

1. The maximum Kmaxwm and minimum nwm reduce the extent of water bound with a matrix and increases the mobility of the FF within a matrix during the period of production, leading to a higher production of FF.
2. The maximum Kmaxwm and minimum nwm also enhance the distribution of FF throughout a matrix during the injection phase, with a better distribution of FF throughout the matrix, a lower S_w in the matrix and, thus, higher P_c values. These elevated P_c values keep a greater amount of FF through the manufacturing process, consequently lowering FF creation.

As shown in Figure 16, the stronger P_c values in Set 30 correspond to lower FF production, consistent with the fact that higher P_c values preserve FF more effectively, reducing FF flowback. Figure 17 plots the GPL, PFF, and cumulative gas to water production proportion (i.e., FGPT/FWPT) for various runs in Set 30, while Figure 18 illustrates that increased FF production results in a higher GPL. This aligns with previous observations for sets with Kmr = 1, where the retained FF within a matrix corresponds with reduced GPL values.

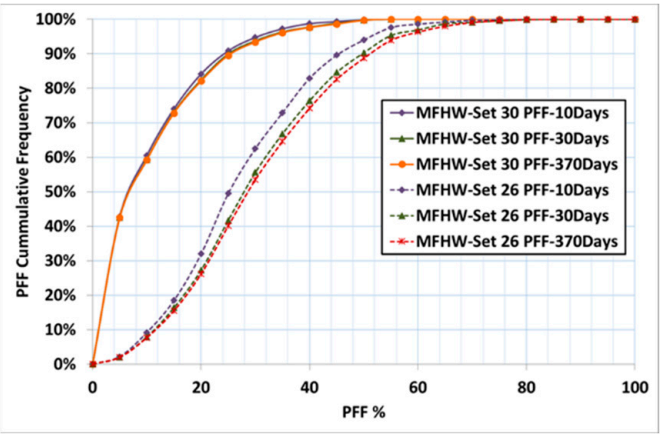

Figure 16. PFF histogram chart of unconventional P_c.

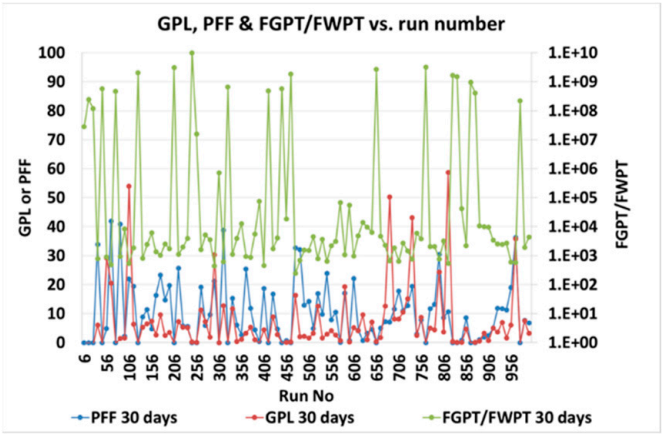

Figure 17. Impact of water retention and flowback on gas production.

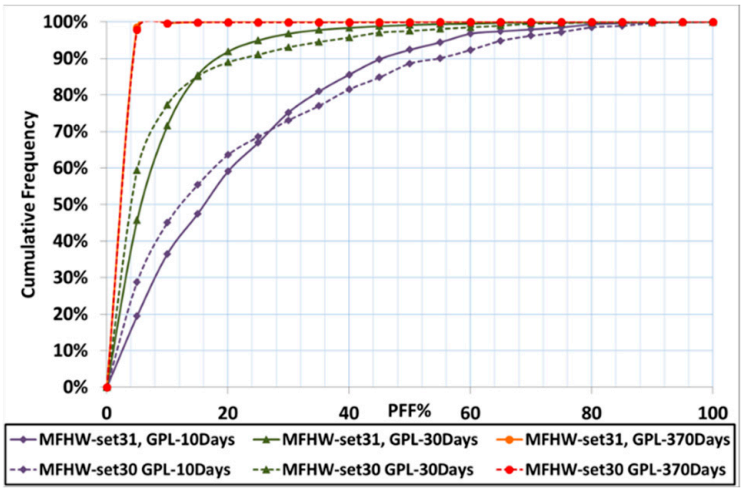

Figure 18. GPL histogram chart of effect of ultra-tight formations.

Investigating these two sets with two approaches towards estimating the P_c highlights that employing IFT reduction chemicals will increase the GPL in sets with tight sand formation.

3.2. Sets Featuring Various Kmr, FVR, and DP Configurations

Therefore, to compare the cleanup efficiency under these unconventional P_c conditions, three additional sets were examined with the Kmr = 100, a significantly increased FVR, and a high DP. The idea was to assess the impact of the given parameters on the cleanup efficacy, bearing in mind an unconventional P_c. Its extension was not incorporated into the subsequent analysis of an unconventional P_c because the results obtained from the analysis of the SFVW and MFVW sets indicated that an extensive ST further enhances FF penetration within a matrix, thus enhancing FF saturation and, at the same time, reducing FF flowback. That, however, appears to be applicable only to the early stages of the production process.

3.3. Low Km Sets with Unconventional P_c

This set was implemented in order to investigate the impact of a remarkably low Km scale (Kmr = 100) on the cleanup efficiency under rather untypical P_c conditions. The Km variation range was cut down from 1 mD to 100 mD in Set 30 to a new range of 0.01 mD–1 mD in this set. From the analysis of the GPL tornado charts for Set 31, in comparison to the highly compact formation presented in Figure 19 and the Set 30 base reference set in Figure 11 that used a different Km range, most of the key parameters had a similar trend, except for the Km factor. In Set 30, a change in Km was seen to change the GPL, with Km significantly effecting the P_c, as depicted in Figure 10. However, in the case of Set 31, there was a negative relationship between Km and the GPL, with an increased value of Km decreasing the GPL, showing the importance of Km to mobility. This shift is attributed to the low permeability characteristics of the rock in this set, which greatly limits the mobility of fluids. The mobility of the fluids within the matrix is more critical here than in Set 30, as previously discussed. The impact of the mobility of the fluids becomes very important following the already high values of the P_c. This can be noted in Figures 18 and 20; the GPL and PFF histograms for the two sets show that the degree of the cleanup outcomes are almost similar, due to the excessive P_c values.

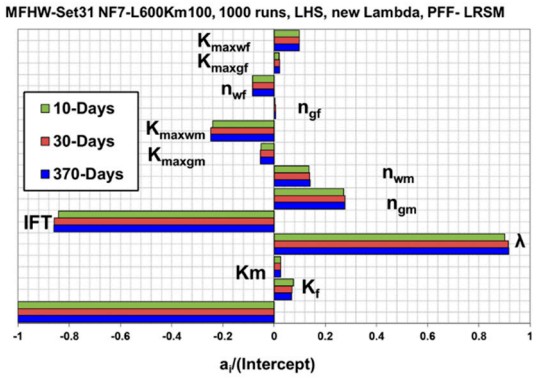

Figure 19. PFF tornado chart of effect of ultra-tight formations.

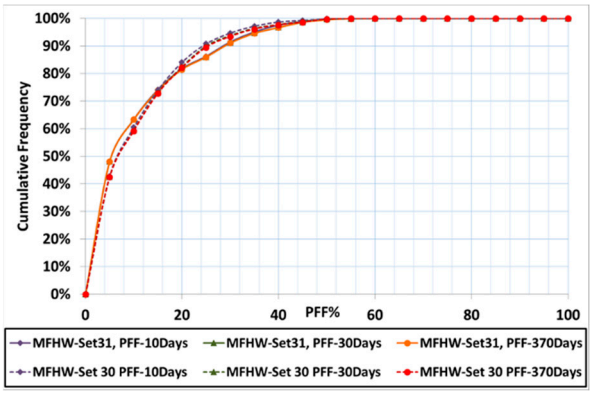

Figure 20. PFF histogram chart of effect of tightness.

When the PFF chart for the ultra-tight Set 31 is compared to the chart for Set 30 base reference set, all the factors described in the tornado chart of Figure 19, except Kf, are similar to those in Figure 12. In Set 31, the Kf primary effect is higher, while in Set 30 the secondary effect of Kf is considered.

A comparison of the sets with unconventional formations highlights that employing IFT reduction chemicals will increase the GPL in sets with tight sand formation (with Km variation ranges of 1 μD–100 μD and 0.1 μD–10 μD). In contrast, employing such substances to decrease the P_c and subsequently lessen the GPL in ultra-tight plays (i.e., km range of 0.01 μD–1 μD) is advised. In essence, it has been established that incorporating IFT (interfacial tension)-reducing agents into fracturing fluids is not advisable in tight formations due to its adverse effect on gas production. However, ultra-tight formations benefit greatly from it since it increases the gas rate.

3.4. Higher FF Volume Sets with Unconventional P_c

This set was created to determine the effect of enhancing the FVR from 2 in Set 30 to 10 on the cleanup efficiency under unconventional P_c conditions. When comparing the GPL tornado chart for Set 32 with an FVR = 10 (Figure 21) with the Set 30 base reference set (Figure 10), which incorporates adjustments to the FF injection during the injection phase, similar trends were observed for all the corresponding parameters of both charts. Furthermore, the following observations were made:

1. In this set, the impact of fluid mobility within the matrix and the fracture on the GPL were more notable in relation to the base reference set.
2. The absolute values of all 12 relevant parameters at one year of production were still high; this means that the cleanup process is significantly longer (up to a year) compared to the duration set by the MFHW, at 30.

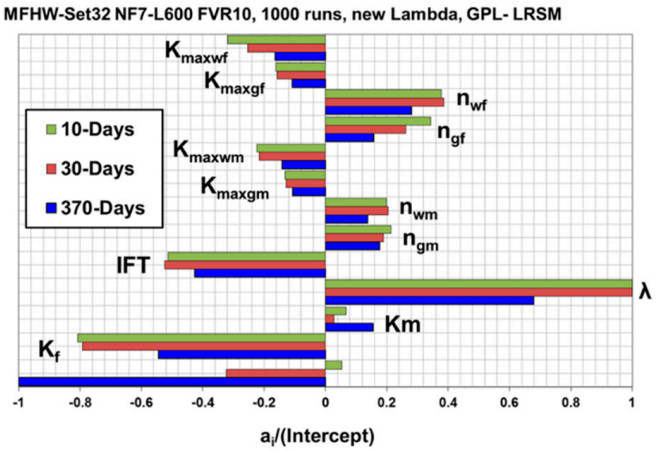

Figure 21. GPL tornado chart of effect of FF volume.

These are due to the fact that the total FF volume introduced in this set is significantly larger. Figure 22 also displays that the cleanup task for the high FVR configuration takes a longer time. From Figure 23, the PFF tornado chart considering the data from Set 32, it can be observed that the initial change predominantly influenced the Kf for the FF production.

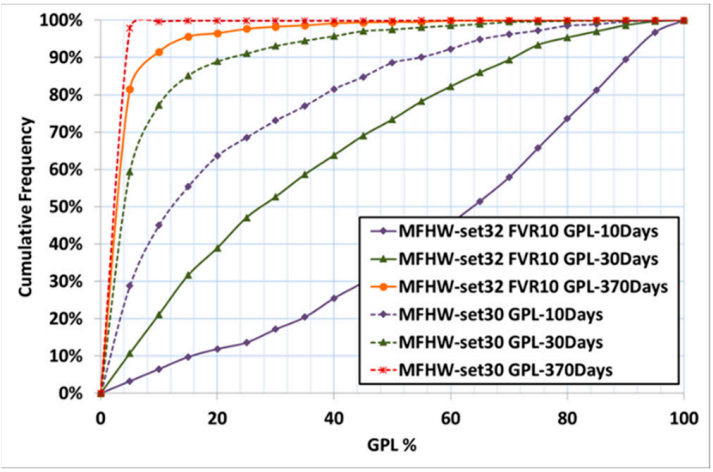

Figure 22. GPL histogram chart of effect of FF volume.

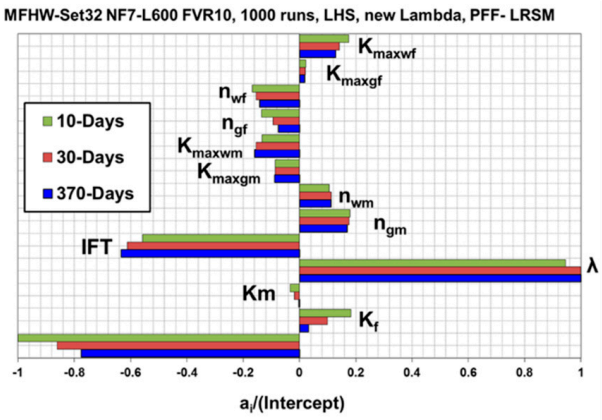

Figure 23. PFF tornado chart of effect of FF volume.

Figure 24 provides the histogram of the PFF for Set 30 (FVR = 2) and Set 32 (FVR = 10). Notably, the cumulative frequency curves of Set 32 during the three production stages do

not overlay one on another, unlike the Set 30 results, suggesting that FF manufacturing goes on for one year.

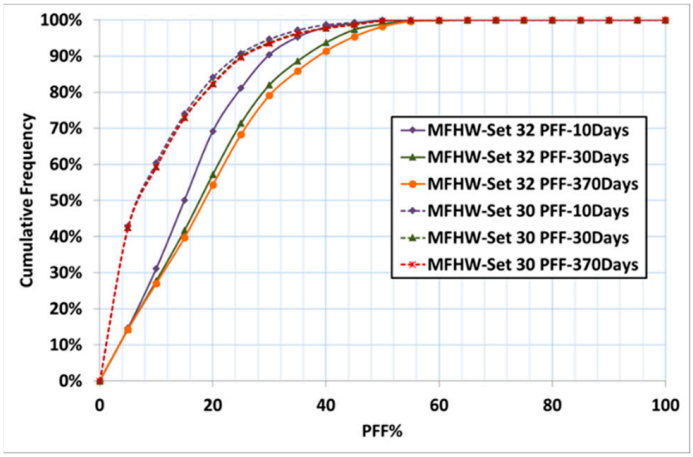

Figure 24. PFF histogram chart of effect of FF volume.

3.5. Impact of Increased Pressure Drawdown and Unconventional P_c

This set was created to capture the effect of a DP increase, with a new P_c, on the cleanup efficiency (the DP was raised from 1000 in Set 30 to 4000 in this set). Using the GPL tornado chart for Set 33 (DP = 4000, Figure 25) with the GPL tornado chart for the Set 30 base reference set (Figure 10), all the significant parameters showed the same trend as the DP was changed from its earlier value. Notably, the impact of the Λ, IFT, and Km on the cumulative gas loss was marginally less pronounced in Set 33 compared to Set 30, due to the increased viscous force, i.e., the higher DP, which made it more challenging to retain FF within the matrix. The influence of Kf on the FF flowback was minimal given the high DP applied in this set (Figure 25).

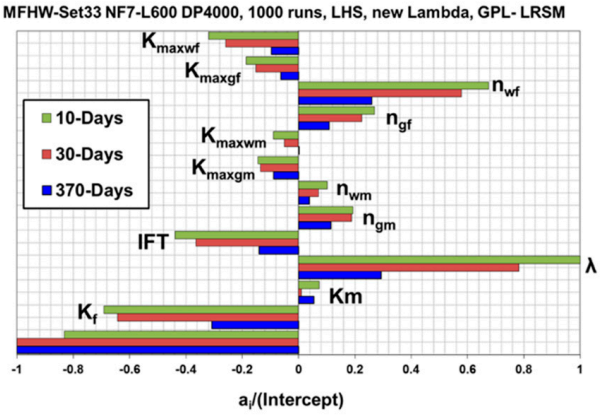

Figure 25. GPL tornado chart showing impact of pressure drawdown.

Figures 26–28 indicate that the larger DP did not expedite the cleanup process in this configuration with an unconventional capillary pressure model. While a higher DP typically enhances cleanup efficiency in the fracture and adjacent matrix, it raises the rate of FF flowback from areas further from the fracture and from inside the matrix at greater depths, which is not beneficial in terms of the cleanup. This amplified FF flowback is illustrated in Figure 28. The balancing effect of these two opposing influences results in a nearly identical cleanup performance across both sets.

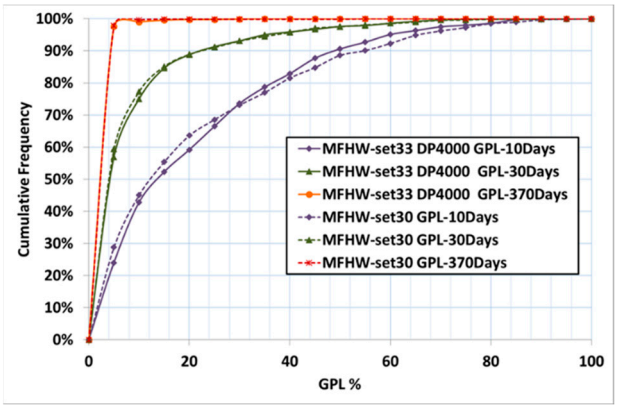

Figure 26. GPL histogram chart showing impact of pressure drawdown.

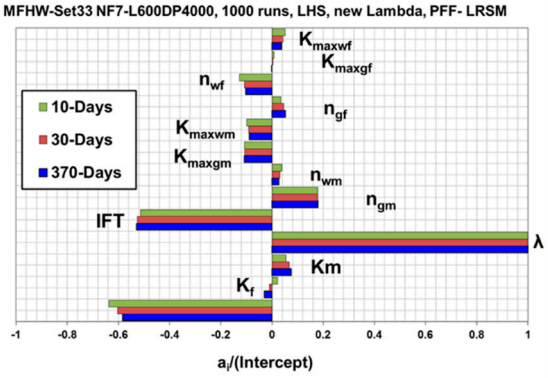

Figure 27. PFF tornado chart showing impact of pressure drawdown.

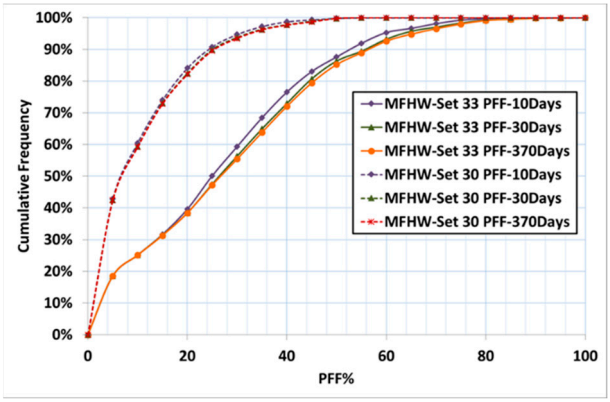

Figure 28. PFF histogram showing impact of pressure drawdown.

4. Conclusions

This work aimed to enhance the comprehension of recent HF treatments for practical field usage by building upon previous research conducted by Nasriani and Jamiolahmady (2019) [29], Nasriani and Jamiolahmady (2018a and b) [30,34], and Nasriani et al. (2018) [36]. The present study sought to investigate the effects of an unconventional P_c on the cleanup effectiveness of MFHWs. For this reason, the assessment of the P_c correlations presented in the current paper for tight and ultra-tight formations used Geo2Flow software.

For these five sets, a new term, analogous to the dimensionless GPL, was incorporated to depict the influence of the relevant parameters on FF production—an aspect critical to the HF of unconventional reservoirs. Outlined below are the principal findings and conclusions of this work:

1. The analyses of the P_c models, based on 200 sets of conventional and unconventional P_c data, revealed that the Brooks and Corey model can be used as a simple, one-parameter P_c model that adequately describes the P_c data for nonconventional formations.
2. On this basis, this research suggests that the λ range should be limited to a range of 0.3–1.5 for a better characterisation of unconventional tight and ultra-tight rocks. These changes were integrated into the model to reflect the unconventional P_c in the new range indicated below.
3. As mentioned earlier, this work found a concave-down section in a few P_c curves due to the dead volume in the P_c determination. Dead volume corrections are therefore important because these errors should not be confused with changes in the inherent properties of the rocks.
4. As expected, various P_c-related parameters, specifically the Λ, substantially affected the GPL in all the sets with a P_c that was adjusted for unconventional cases. This can be attributed to the difference in the λ variation range identified in the unconventional P_c sets, which caused the P_c to be more sensitive than in the conventional sets.
5. Kf influenced FF production in two distinct ways:
    - A higher Kf improved FF mobility within the fractured region during the production phase, leading to increased FF production.
    - Higher values of Kf also promoted increased FF mobility within the fracture region throughout the injection phase, and also provided a better distribution of the FF in the fracture, a lower saturation (S_w) in the matrix phase, and higher P_c values. These higher P_c values maintained a greater proportion of the FF during production and, thus, a lower FF.
6. The PFF tornado charts indicated a decline in FF production as the water mobility within the matrix increased. This outcome is due to the dual impact of the matrix water mobility on FF production:
    - More FF is produced during the production stage when there is greater matrix water mobility, which improves the FF mobility inside the matrix.
    - Greater FF matrix mobility throughout the injection phase is a result of more substantial water mobility in the matrix; this leads to more dispersed FF, lower matrix S_w values, and higher P_c values. Higher P_c values produce less FF because they retain more FF during backflow.
7. When the same sets were exposed to a reduced Km or an increased injected FF volume to FVR for the sets using an unconventional P_c, the outcomes were similar to when a conventional P_c was used. The primary ones are as follows:
    a. It was only after bringing down the Km range or increasing the FVR that the cleanup was significantly hampered.
    b. However, in the set with Kmr = 1, the Km coefficient was positive, suggesting that an increase in Km raised the GPL. This suggests that the Km effect, which reduces the value of the P_c and increases the output of the FF, is critical. In the set with Kmr = 100, the Km coefficient was negative; therefore, an increase in Km led to a decline in the GPL. This implies that Km actually has a great influence on the mobility of the matrix. The cause of this change in the trend is that the rock in this set is very consolidated, and thus makes matrix fluid movement practically impossible.
    c. These are asymptotic and numerical values illustrating the impact of fluid mobility on the GPL for the set with a higher FVR than the set with a lower FVR.
8. As mentioned before, the cleanup process in the set with an atypical PC was not accelerated by the augmentation of the DP. This is because, as described earlier, while increasing the DP accelerated the cleanup in the fracture and the vicinity of the matrix surrounding the fracture, at some distance away from the fracture the repairs were faster and reduced flowback from deeper FF zones in the matrix. These two impacts tended to cancel each other out and the sets with standard and unusual P_c curves

revealed a cleaner output with comparable efficiency. The higher viscous force led to a higher FF flowback in the relevant set, and that is why there was a higher FF flowback in this high DP set with an atypical P_c. But the interaction of most of the FF flowback with a conventional PC was found for a moderate value of the DP.

i. A stronger viscous force led to the formation of more FF flowback in the relevant set, and that is why there was more FF flowback in this high DP set with an executive pressure coefficient that deviated from the norm. However, since a conventional P_c does not have as significant a P_c value as an unconventional P_c to continue to keep the FF inside the matrix, most of the flowback occurred at moderate values for the DP.

9. A comparison of the sets of tight and ultra-tight formations highlights that employing IFT reduction chemicals will increase the GPL in sets with tight sand formation (with Km variation ranges of 1 μD–100 μD and 0.1 μD–10 μD). In contrast, employing such substances to decrease the P_c and subsequently lessen the GPL in ultra-tight plays (i.e., km range of 0.01 μD–1 μD) is advised. To put it differently, this study has established that incorporating IFT-reducing agents into fracturing fluids negatively impacts gas production rates in tight formations, but is highly beneficial in ultra-tight formations as it increases production rates.

- The wastewater or flowback fluid that returns from a well is expected to have high concentrations of naturally occurring minerals and metals that have dissolved into the water from the shale and other rock formations.
- Additionally, a small amount of the non-hazardous chemicals injected during the fracturing process and naturally occurring radioactive materials (NORMs) may be present in the fluid. Therefore, this conclusion is environmentally significant. Consequently, it is strongly advised against using IFT-reducing agents in tight formations to aid the matrix in imbibing most of the FF and minimising flowback.

Author Contributions: Conceptualization, H.R.N.; Methodology, H.R.N. and M.J.; Software, H.R.N.; Validation, H.R.N.; Formal analysis, H.R.N.; Investigation, H.R.N.; Resources, H.R.N.; Data curation, H.R.N.; Writing—original draft, H.R.N.; Writing—review & editing, H.R.N.; Supervision, M.J. All authors have read and agreed to the published version of the manuscript.

Funding: This research received no external funding.

Data Availability Statement: The original contributions presented in the study are included in the article, further inquiries can be directed to the corresponding author.

Conflicts of Interest: The authors declare no conflict of interest.

References

1. The U.S. Energy Information Administration (EIA). Natural Gas. Available online: https://www.eia.gov/naturalgas/data.php (accessed on 21 February 2024).
2. International Energy Agency. *Gas Market Report, Q3-2024*; International Energy Agency: Paris, France, 2024.
3. Enbridge, Energy Matters Enbridge Is Natural Gas Environmentally Friendly? 2024. Available online: https://www.enbridge.com/energy-matters/energy-school/natgas-enviro-friendly#:~:text=Natural%20gas%20produces%20less%20pollution,15%20percent%20less%20than%20wood (accessed on 21 February 2024).
4. Campin, D. Environmental Regulation of Hydraulic Fracturing. *SPE Prod. Oper.* **2015**, *30*, 329–361. [CrossRef]
5. Chen, B.; Barboza, B.R.; Sun, Y.; Bai, J.; Thomas, H.R.; Dutko, M.; Cottrell, M.; Li, C. A Review of Hydraulic Fracturing Simulation. *Arch. Comput. Methods Eng.* **2021**, *29*, 1–58. [CrossRef]
6. Yu, H.; Xu, W.; Li, B.; Huang, H.; Micheal, M.; Wang, Q.; Huang, M.; Meng, S.; Liu, H.; Wu, H. Hydraulic Fracturing and Enhanced Recovery in Shale Reservoirs: Theoretical Analysis to Engineering Applications. *Energy Fuels* **2023**, *37*, 9956–9997. [CrossRef]
7. Davoodi, S.; Al-Shargabi, M.; Wood, D.A.; Rukavishnikov, V.S. A Comprehensive Review of Beneficial Applications of Viscoelastic Surfactants in Wellbore Hydraulic Fracturing Fluids. *Fuel* **2023**, *338*, 127228. [CrossRef]
8. Osiptsov, A.A. Fluid Mechanics of Hydraulic Fracturing: A Review. *J. Pet. Sci. Eng.* **2017**, *156*, 513–535. [CrossRef]
9. Bennion, D.B.; Thomas, F.B.; Ma, T. Recent Advances in Laboratory Test Protocols to Evaluate Optimum Drilling, Completion and Stimulation Practices for Low Permeability Gas Reservoirs. In Proceedings of the SPE Rocky Mountain Petroleum Technology Conference/Low-Permeability Reservoirs Symposium, Denver, CO, USA, 12–15 March 2000.

10. Zhao, J.; Ren, L.; Jiang, T.; Hu, D.; Wu, L.; Wu, J.; Yin, C.; Li, Y.; Hu, Y.; Lin, R. Ten Years of Gas Shale Fracturing in China: Review and Prospect. *Nat. Gas Ind. B* **2022**, *9*, 158–175. [CrossRef]
11. Bin, Y.; Mingze, Z.; Siwei, M.; Zhang, W.; Zheng, H. Intelligent Identification and Real-Time Warning Method of Diverse Complex Events in Horizontal Well Fracturing. *Pet. Explor. Dev.* **2023**, *50*, 1487–1496.
12. Qun, L.E.I.; Yun, X.U.; Bo, C.A.I.; Baoshan, G.; Xin, W.; Guoqiang, B.I.; Hui, L.I.; Shuai, L.I.; Bin, D.; Haifeng, F.U. Progress and Prospects of Horizontal Well Fracturing Technology for Shale Oil and Gas Reservoirs. *Pet. Explor. Dev.* **2022**, *49*, 191–199.
13. Nianyin, L.; Jiajie, Y.; Chao, W.; Suiwang, Z.; Xiangke, L.; Jia, K.; Yuan, W.; Yinhong, D. Fracturing Technology with Carbon Dioxide: A Review. *J. Pet. Sci. Eng.* **2021**, *205*, 108793. [CrossRef]
14. Dong, Z.; Holditch, S.A.; McVay, D.; Ayers, W.B. Global Unconventional Gas Resource Assessments. *SPE Econ. Manag.* **2011**, *4*, 222–234. [CrossRef]
15. Niu, W.; Sun, Y.; Zhang, X.; Lu, J.; Liu, H.; Li, Q.; Mu, Y. An Ensemble Transfer Learning Strategy for Production Prediction of Shale Gas Wells. *Energy* **2023**, *275*, 127443. [CrossRef]
16. Guo, J.; Lu, Q.; He, Y. Key Issues and Explorations in Shale Gas Fracturing. *Nat. Gas Ind. B* **2023**, *10*, 183–197. [CrossRef]
17. Shen, W.; Ma, T.; Zuo, L.; Yang, X.; Cai, J. Advances and Prospects of Supercritical CO2 for Shale Gas Extraction and Geological Sequestration in Gas Shale Reservoirs. *Energy Fuels* **2024**, *38*, 789–805. [CrossRef]
18. He, X.; Chen, G.; Wu, J.; Liu, Y.; Wu, S.; Zhang, J.; Zhang, X. Deep Shale Gas Exploration and Development in the Southern Sichuan Basin: New Progress and Challenges. *Nat. Gas Ind. B* **2023**, *10*, 32–43. [CrossRef]
19. Niu, W.; Lu, J.; Sun, Y.; Liu, H.; Cao, X.; Zhan, H.; Zhang, J. A Review of the Application of Data-Driven Technology in Shale Gas Production Evaluation. *Energy Rep.* **2023**, *10*, 213–227. [CrossRef]
20. Li, H. Coordinated Development of Shale Gas Benefit Exploitation and Ecological Environmental Conservation in China: A Mini Review. *Front. Ecol. Evol.* **2023**, *11*, 1232395. [CrossRef]
21. Clark, J.B. A Hydraulic Process for Increasing the Productivity of Wells. *J. Pet. Technol.* **1949**, *1*, 1–8. [CrossRef]
22. Suboyin, A.; Rahman, M.M.; Haroun, M. Hydraulic fracturing design considerations, water management challenges and insights for Middle Eastern shale gas reservoirs. *Energy Rep.* **2020**, *6*, 745–760. [CrossRef]
23. Height, B.C. Process of Increasing Permeability of Sands and Strata. U.S. Patent No. 2,354,570, 25 July 1944.
24. Lee, R.E. Method of Treating a Producing Formation 1939. Available online: https://patents.google.com/patent/US2171416A/en (accessed on 21 February 2024).
25. Holditch, S.A. Factors Affecting Water Blocking and Gas Flow From Hydraulically Fractured Gas Wells. *J. Pet. Technol.* **1979**, *31*, 1515–1524. [CrossRef]
26. Montgomery, K.T.; Holditch, S.A.; Berthelot, J.M. Effects of Fracture Fluid Invasion on Cleanup Behavior and Pressure Buildup Analysis. In Proceedings of the SPE Annual Technical Conference and Exhibition, New Orleans, Louisiana, 23–26 September 1990; pp. 279–290.
27. Pope, D.; Britt, L.K.; Constien, V.; Anderson, A.; Leung, L. Field Study of Guar Removal from Hydraulic Fractures. In Proceedings of the SPE Formation Damage Control Symposium, Lafayette, LA, USA, 14–15 February 1996; pp. 1–7. [CrossRef]
28. Gdanski, R.D.; Weaver, J.; Slabaugh, B.; Walters, H.; Parker, M. SPE 94649 Fracture Face Damage—It Matters. In Proceedings of the SPE European Formation Damage Conference, Sheveningen, The Netherlands, 25–27 May 2005.
29. Nasriani, H.R.; Jamiolahmady, M. Flowback Cleanup Mechanisms of Post-Hydraulic Fracturing in Unconventional Natural Gas Reservoirs. *J. Nat. Gas Sci. Eng.* **2019**, *66*, 316–342. [CrossRef]
30. Nasriani, H.R.; Jamiolahmady, M. Maximizing Fracture Productivity in Unconventional Fields; Analysis of Post Hydraulic Fracturing Flowback Cleanup. *J. Nat. Gas Sci. Eng.* **2018**, *52*, 529–548. [CrossRef]
31. Tech-Flo Consulting. Available online: https://www.tech-flo.net/frac-flowback.html (accessed on 1 February 2024).
32. Halliburton. Available online: https://www.halliburton.com/en-US/ps/testing-subsea/reservoir-testing-analysis/calibr.html?node-id=i4msmulo (accessed on 1 February 2024).
33. Ghahri, P. Modelling of Gas-Condensate Flow around Horizontal and Deviated Wells and Cleanup Efficiency of Hydraulically Fractured Wells. Ph.D. Thesis, Heriot-Watt University, Edinburgh, UK, 2010. Available online: https://www.ros.hw.ac.uk/handle/10399/2354 (accessed on 1 February 2024).
34. Nasriani, H.R.; Jamiolahmady, M. A Comparison of Clean-Up Efficiency of Multiple Fractured Horizontal Wells and Hydraulically Fractured Vertical Wells in Tight Gas Reservoirs. In Proceedings of the SPE Europec featured at 80th EAGE Conference and Exhibition; Society of Petroleum Engineers, Copenhagen, Denmark, 11–14 June 2018.
35. Nasriani, H.R.; Jamiolahmady, M.; Alajmi, E. An Integrated Study of Cleanup Efficiency of Short Hydraulic Fractured Vertical Wells Using Response Surface Methodology. In Proceedings of the 76th EAGE Conference and Exhibition 2014, Amsterdam, The Netherlands, 16–19 June 2014.
36. Nasriani, H.R.; Jamiolahmady, M.; Saif, T.; Sánchez, J. A Systematic Investigation into the Flowback Cleanup of Hydraulic-Fractured Wells in Unconventional Gas Plays. *Int. J. Coal. Geol.* **2018**, *193*, 46–60. [CrossRef]
37. Nasriani, H.R.; Jamiolahmady, M.; Alajmi, E.; Ghahri, P. A Study of Hydraulic Fracturing Clean-up Efficiency in Unconventional Gas Reservoirs Using Statistical Approaches. In Proceedings of the ECMOR XIV-14th European Conference on the Mathematics of Oil Recovery, Catania, Italy, 8–11 September 2014.
38. Nasriani, H.R.; Borazjani, A.A.; Iraji, B.; MoradiDowlatAbad, M. Investigation into the Effect of Capillary Number on Productivity of a Lean Gas Condensate Reservoir. *J. Pet. Sci. Eng.* **2015**, *135*, 384–390. [CrossRef]

39. Nasriani, H.R.; Borazjani, A.A.; Sinaei, M.; Hashemi, A. The Effect of Gas Injection on the Enhancement of Condensate Recovery in Gas Condensate Reservoirs: A Comparison between a Synthetic Model and PVT Cell Results. *Pet. Sci. Technol.* **2014**, *32*, 596890. [CrossRef]
40. Modebelu, E.C.; Nasriani, H.R.; Francis, J. Integrated Evaluation of the Clean-Up Performance of Unconventional Gas Plays; Investigating the Impact of Desiccation. In Proceedings of the 83rd EAGE Annual Conference & Exhibition; European Association of Geoscientists & Engineers, Madrid, Spain, 6–9 June 2022; pp. 1–5.
41. Erimako, R.J.B.; Nasriani, H.R.; Asimakopoulou, E.; Graham, T.L.; Whitty, J. Numerical Investigation of Hydraulic Fractures in Multiple Horizontal Wells: Analysis of Zipper & Modified Zipper Fracking. In Proceedings of the 83rd EAGE Annual Conference & Exhibition; European Association of Geoscientists & Engineers, Madrid, Spain, 6–9 June 2022; pp. 1–5.
42. Shi, Z.; Huang, Y.; Flottman, T.; Leonardi, C.; Lu, M.; Chen, Z. Characterization of Anisotropic Geomechanical Properties of Australian Bowen Basin Coals Through Nanoindentation and Upscaling Approaches. In Proceedings of the SPE Asia Pacific Unconventional Resources Conference and Exhibition, Brisbane, Australia, 14–15 November 2023.
43. Leonardi, C.R.; Di Vaira, N.J.; Laniewski-Wollk, L.; Ganpule, S.; Flottmann, T. Computational Analysis of Proppant Transport and Screen-Out in Natural and Induced Fractures. In Proceedings of the SPE Asia Pacific Unconventional Resources Conference and Exhibition, Brisbane, Australia, 14–15 November 2023.
44. Awan, F.U.R.; Keshavarz, A.; Akhondzadeh, H.; Al-Anssari, S.; Al-Yaseri, A.; Nosrati, A.; Ali, M.; Iglauer, S. Stable Dispersion of Coal Fines during Hydraulic Fracturing Flowback in Coal Seam Gas Reservoirs—An Experimental Study. *Energy Fuels* **2020**, *34*, 5566–5577. [CrossRef]
45. Leonardi, C.R.; Di Vaira, N.J.; Laniewski-Wollk, L.; Aminossadati, S.M.; Johnson, R.L. Probabilistic Quantification of Size Segregation and Screen-Out of Microparticles Subject to Electrostatic Forces. In Proceedings of the SPE Hydraulic Fracturing Technology Conference and Exhibition, The Woodlands, TX, USA, 31 January–2 February 2023.
46. Ramanandraibe, H.M.; Johnson, R.L.; Sedaghat, M.; Leonardi, C.R. Co-Application of Indirect Hydraulic Fracturing and Micro-Proppants with Existing Surface-to-Inseam Wells to Improve Pre-Drainage of Low Permeability Coals in Mining Areas. In Proceedings of the Abu Dhabi International Petroleum Exhibition and Conference, Abu Dhabi, United Arab Emirates, 2–5 October 2023.
47. Srinivasan, S.; O'Malley, D.; Mudunuru, M.K.; Sweeney, M.R.; Hyman, J.D.; Karra, S.; Frash, L.; Carey, J.W.; Gross, M.R.; Guthrie, G.D.; et al. A Machine Learning Framework for Rapid Forecasting and History Matching in Unconventional Reservoirs. *Sci. Rep.* **2021**, *11*, 21730. [CrossRef]
48. O'Meara Consulting Inc. *Geo2Flow*; Release 4 May 2014; O'Meara Consulting Inc.: Cedar Rapids, IA, USA, 2014.
49. Leverett, M. Capillary behavior in porous solids. *Trans. AIME* **1941**, *142*, 152–169. [CrossRef]
50. Brooks, R.H.; Corey, A.T. *Hydraulic Properties of Porous Media*; Colorado State University: Fort Collins, CO, USA, 1964.
51. Brooks, R.H.; Corey, A.T. Properties of Porous Media Affecting Fluid Flow. *J. Irrig. Drain. Div.* **1966**, *92*, 61–90. [CrossRef]
52. Bentsen, R.G.; Anli, J. Using Parameter Estimation Techniques To Convert Centrifuge Data Into a Capillary-Pressure Curve. *Soc. Pet. Eng. J.* **1977**, *17*, 57–64. [CrossRef]
53. Shafer, J.; Neasham, J. Mercury porosimetry protocol for rapid determination of petrophysical and reservoir quality properties. In *International Symposium of the Society of Core Analysts*; Society for Core Analysts: Fredericton, NB, Canada, 2000; pp. 18–22.
54. Schlumberger Geoquest. *ECLIPSE 100*, Version 2015.1.0.0; Simulation Launch Management Utility; Schlumberger Geoquest: Houston, TX, USA, 2015.
55. Thomas, L.K.; Katz, D.L.; Tek, M.R. Threshold Pressure Phenomena in Porous Media. *Soc. Pet. Eng. J.* **1968**, *8*, 174–184. [CrossRef]